

Frequency-based current differential protection for VSC-MVDC distribution lines

Meng Li^a, Yiping Luo^a, Ke Jia^{b,*}, Tianshu Bi^b, Qixun Yang^b

^a School of Electrical Engineering, Beijing Jiaotong University, Beijing, People's Republic of China

^b State Key Laboratory of Alternate Electrical Power System with Renewable Energy Sources, North China Electric Power University, Beijing, People's Republic of China

ARTICLE INFO

Keywords:

Current differential protection
Direct current
Frequency dominion
Discrete Wavelet Transform
Mother wavelet selection

ABSTRACT

The current of line distributed capacitance might affect the performance of current differential protection, which becomes more serious in DC systems. This paper proposes the frequency-based current differential protection for VSC-MVDC distribution lines to solve the above problem. The protection identifies internal faults using the ratio of low-frequency energy to high-frequency energy of the differential current. Unlike the existing current differential protection, the proposed protection: (1) is not disturbed by the current of the line distributed capacitance that is the brake component instead of the maloperation component to the proposed protection; (2) can tolerate the interference of the noise that is high-frequency. The protection criteria are presented, and the settings are analysed. The dead zone component is proposed to handle near-end faults. The test results have shown that the proposed protection is not affected by the line-distributed capacitance and can correctly operate under 50 Ω fault resistance. It can also tolerate 20 dB of white noise and 40 μ s of synchronisation error.

1. Introduction

With the development of the renewable distributed generations and DC loads, VSC (Voltage Source Converter)-MVDC (Medium Voltage Direct Current) distribution systems [1] have been researched for their excellent performance in areas such as fewer conversion stages for both distributed generations and DC loads, flexible control, excellent power quality, etc. Although the VSCs can limit AC fault current, they are vulnerable to DC faults [2,3]. The DC faults will cause serious overcurrent with the peak usually attained within a couple of milliseconds. Even though the VSC is blocked, the fault current can still flow through the diodes of VSC, and the overcurrent cannot be eliminated [4]. The DC circuit breaker (DCCB) [5] is a promising candidate for MVDC distribution networks. DC line protections (the scope of this paper) are crucial to the DCCB scheme.

The high speed and selectivity are expected for the DC line protections. The high speed (a couple of milliseconds) can prevent VSCs from being damaged and also brings down the interrupting requirement of DCCB. The selectivity of protection can isolate the fault line without interruption of the continuous operation of adjacent healthy lines, which is significant to the power supply reliability. The existing literatures have proposed some protection algorithms but have some shortcomings.

The travelling wave protection [6] is generally adopted as a primary

protection in the traditional HVDC (High Voltage Direct Current) systems with LCC (Line Commuted Converter). Refs. [7,8] introduce the travelling wave protections into VSC-DC systems. The Ref. [7] adopts the wave shape properties of the first travelling wave, which is independent of the arrival times. However, the data acquisition units with very high sampling rate is necessary. The Ref. [8] proposes a novel protection based on the surge arrival time difference between the ground-mode and line-mode travelling waves. Nevertheless, the method is only suitable for pole-to-ground faults, and cannot be used for pole-to-pole faults without the ground-mode travelling waves.

Current protections are proposed in [9,10]. However, the setting calculation in instantaneous value is a challenge in [9]. The method in [10] is suitable for the DC microgrid, in which there is no segmentation on lines. A passive circuit is introduced to assist the current protection in identifying high resistance faults in [11]. The added circuit could adversely affect the system reliability. Ref. [12] researches the directional current protection scheme for LVDC grids, which is difficult to apply to the MVDC distribution network. The protections based on the change rate of voltage [13] and current [14] are researched, which are vulnerable to fault resistances and high-frequency noises [15]. A distance protection [16] calculates the fault distance with the voltage difference between two voltage sensors. This method needs an extra sensor. Additionally, the above local-measurement protections are difficult to protect the whole line at a satisfactory speed.

* Corresponding author.

E-mail address: ke.jia@ncepu.edu.cn (K. Jia).

The fault current limiting reactors can be considered as the boundary to high-frequency components. Some boundary protections are proposed to achieve the selectivity requirement using the voltages on both sides of the limiting reactor [17], their changing rates [18], and the changing rate of the limiting reactor voltage [19]. However, these reactors may adversely affect the dynamic performance of control and reduce the voltage stability of the system [20]. Additionally, the boundary protections cannot be utilised in the system without DC-limiting reactors at the both terminals of the lines.

The current differential protections can protect the whole line for the system without DC-limiting reactors, which is widely adopted in AC and DC systems. However, because of the line distributed capacitance (LDC), the current differential protection in the LCC-HVDC systems generally needs a large time-delay to avoid maloperation [21]. The current differential protections [22–24] are applied for low voltage VSC-DC microgrids in which the LDC is not considerable. In the VSC-MVDC distribution system, the cables of several kilometres are involved, and the LDC cannot be ignored. The current differential protection will be a potential primary protection for the VSC-MVDC distribution system if the problem of the LDC can be adequately solved.

In AC systems, capacitance current compensation algorithms based on π -type line model [25] and the steady state transmission line model [26] have been researched to improve the performance of current differential protections. However, the transient current of LDC cannot be completely compensated, which is the main problem for the current differential protections of DC systems. A differential protection based on equivalent travelling wave [27] is proposed for the AC system. Although the protection can tolerate the interference of LDC, the high sampling rate is adopted. In [28], a transverse differential current protection is proposed for pole-to-ground faults, which is immune to the LDC. However, the protection becomes invalid for pole-to-pole faults. The existing methods are still unable to solve the problem of the LDC transient current thoroughly.

Aiming at the problem of the LDC transient current, this paper proposed a novel current differential protection that is based on the frequency instead of magnitude. The protection identifies internal faults using the ratio of low-frequency energy to high-frequency energy of the differential current, which is immune to the LDC current thoroughly and can tolerate the interference of the noise that is high-frequency. The Discrete Wavelet Transform (DWT) is adopted to extract the frequency characteristic of the differential current. A dead zone criterion is proposed to assist the protection in handling near-end faults.

2. Characteristics of differential current

The research object of this paper is shown in Fig. 1. The rated voltage of the DC distribution network is ± 10 kV. It consists of two terminals interfaced with AC sources through VSC1 and VSC2. The DC load and the AC load are respectively connected through the DC transformer and VSC3. The diodes at the load connection points are used to avoid fluctuations of load voltage during DC line faults. DC circuit breakers are configured to test the selectivity of the proposed protection.

Classical VSC topologies involve the two-level VSC [29] and MMC (Modular Multilevel Converter) [30]. Because the voltage level of DC distribution networks is relatively low, the two-level VSC is adopted in the research object.

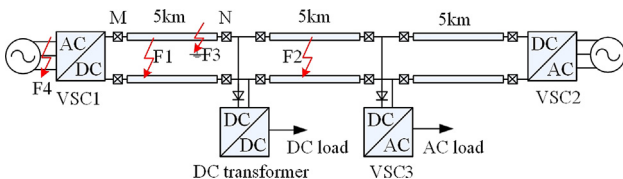


Fig. 1. Schematic diagram of DC distribution system.

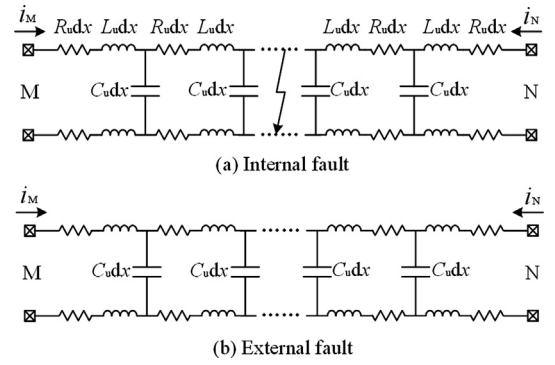


Fig. 2. Equivalent circuits of line with distributed parameters.

The equivalent circuit of line with distributed parameters is shown in Fig. 2. The differential current is equal to the sum of the currents at both ends (i_M and i_N in Fig. 2). For the internal fault (Fig. 2a), the differential current includes fault currents and LDC currents. For the external fault (Fig. 2b), the differential current only includes and LDC currents.

In the case of internal or external faults, there are significant differences in the main components of the differential current. Therefore, if the differences can be extracted and scaled, the internal and external faults can be discriminated. The frequency characteristics of fault currents and LDC currents will be respectively analysed as follows.

2.1. Frequency characteristics of fault current

For two-level VSC, the fault process of DC pole-to-pole faults can be divided into three stages [31], namely, the DC-linked capacitor “discharging stage”, diode “free-wheeling stage” and AC-side current “feeding stage”, as shown in Fig. 3. The frequency characteristics of the current during each stage are analysed, respectively, as follows.

2.1.1. Discharging stage

After the fault inception, the DC-linked capacitor firstly discharges to the fault point. During this stage, the line fault current mainly concludes the discharging current of the DC-linked capacitor. The AC system has less impact on the fault current in the stage. Therefore, the equivalent circuit can be simplified to a second-order circuit as shown

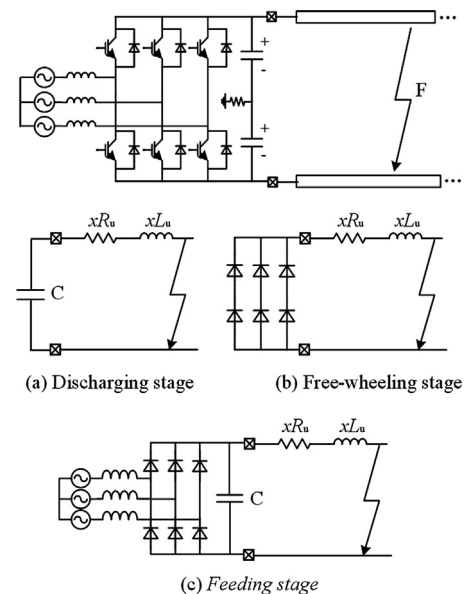


Fig. 3. Equivalent circuits in different stages.

in Fig. 3(a). The main component of the fault circuit is the decaying periodic component whose frequency can be calculated with the Eq. (1):

$$f = \frac{\sqrt{(1/dL_u C) - (R_u/2L_u)^2}}{2\pi} \quad (1)$$

where d is fault distance, R_u and L_u are resistance and inductance per unit length of the DC line, respectively. C represents capacitance of DC-linked capacitor.

From the above equation, the current frequency is inversely proportional to the fault distance and the capacitance of the DC-linked capacitor. Due to the large capacitance of the DC-linked capacitor, the frequency of the fault current is generally low. With the system parameters of this paper, for a fault occurs at 0.5 km, the frequency of the current is about 875 Hz. When the fault distance is larger, the frequency will be lower. For the faults at near-end, this case will be discussed as a dead zone in Section 3.4.

Therefore, during the discharging stage, the fault current is concentrated in the frequency band of less than 1000 Hz.

2.1.2. Free-wheeling stage

When the DC voltage decays to zero, the fault current flows through the reverse parallel diodes of the converter, which is called the diode free-wheeling stage. The equivalent circuit is a first-order attenuation circuit, as shown in Fig. 3(b). The expression of the fault current is:

$$i_F = I_0 e^{-(R_u/L_u)t} \quad (2)$$

where I_0 is the initial fault current for this stage.

The fault current is a decaying DC component. With the system parameters of this paper, the decay time constant is 2.64 ms. Therefore, during the free-wheeling stage, the main frequency band of fault current is also less than 1000 Hz.

2.1.3. Feeding stage

With the attenuation of the DC fault current, the AC side starts to feed the current to the fault point through the diode rectifier bridge (the locked converter). The equivalent circuit is shown in Fig. 3(c). According to the characteristics of the diode rectifier bridge, the fault current mainly contains DC components and 6th harmonic components [32]. Therefore, the main frequency band of fault current is concentrated below 300 Hz (the AC side power frequency is assumed to be 50 Hz).

In summary, during the entire fault, the fault current is mainly concentrated in the low-frequency band below 1000 Hz.

2.2. Frequency characteristics of LDC current

During the transient stage, the propagation of the fault travelling wave causes a change in voltage. The negative voltage travelling wave causes discharging of LDC, and the positive one causes charging. The frequency of LDC current is related to the polarity of voltage wave, which is analysed as follows.

Taking the positive pole line as an example, after the inception of DC pole-to-pole faults, the polarity of the initial voltage wave from the fault point is negative, and the LDC discharges. The transmission time of the travelling wave from the fault point to the line terminal is τ .

$$\tau = \frac{d}{v} \quad (3)$$

where v is the travelling wave velocity, d is fault distance.

When the travelling wave arrivals the line terminal, the polarity of the reflected voltage wave is determined by the polarity of reflection coefficient β as shown in (4).

$$u_r = \beta \cdot u_i \quad (4)$$

$$\beta_{\text{terminal}} = \frac{z_{\text{terminal}} - z_{\text{line}}}{z_{\text{terminal}} + z_{\text{line}}} \quad (5)$$

where u_r is the reflected voltage wave and u_i is the incident wave; β_{terminal} is the reflection coefficient of line terminal, z_{terminal} is the wave impedance of the terminal, and z_{line} is the wave impedance of the line.

In the first case, the terminal wave impedance is greater than the line wave impedance, and β_{terminal} is positive, and the polarity of reflected voltage wave at the line terminal is still negative. The LDC continues to discharge. After the time of τ , the wave arrivals the fault point. The reflection coefficient of the fault point is

$$\beta_{\text{fault}} = \frac{z_{\text{fault}} - z_{\text{line}}}{z_{\text{fault}} + z_{\text{line}}} \quad (6)$$

where z_{fault} is the wave impedance of fault point where the fault resistance and the line wave impedance are connected in parallel. z_{fault} is less than z_{line} , and β_{fault} is always negative.

Therefore, the reflected voltage wave at the fault point is positive. The LDC charges during the next τ time. Then the wave arrival the line terminal again. The reflected voltage wave at the line terminal is positive (β_{terminal} is positive), and LDC continues to charge during the next τ time. The next process will repeat the above analysis. The whole process is shown in Fig. 4a. The main frequency of LDC current is

$$f_{\text{LDC}} = \frac{1}{4\tau} = \frac{v}{4d} \quad (7)$$

In the second case, the terminal wave impedance is less than the line wave impedance, and β_{terminal} is negative. The travelling wave process is shown in Fig. 4b. The main frequency of LDC current is

$$f_{\text{LDC}} = \frac{1}{2\tau} = \frac{v}{2d} \quad (8)$$

In any case, the frequency of LDC current is above $v/4d$ [33].

It is considered that the distribution distance will not exceed 40 km in ± 10 kV DC distribution networks [34]. Travelling wave velocity is close to the speed of light. It can be calculated that the frequency of LDC current is not less than 1800 Hz.

From the above analysis, for DC pole-to-pole faults, the fault current is mainly concentrated in the low-frequency band below 1000 Hz, and the LDC current is concentrated in the high-frequency band above 1800 Hz. Therefore, by detecting the frequency distribution of the differential current, it is possible to distinguish internal faults from external faults.

3. Frequency-based current differential protection

A new current differential protection is proposed in this paper. Instead of using the magnitude of the differential current, the frequency distribution of the differential current is utilised. The protection algorithm includes a start-up component, a fault-type component, an internal fault identification component and a dead zone component. These components and protection logic are presented as follows.

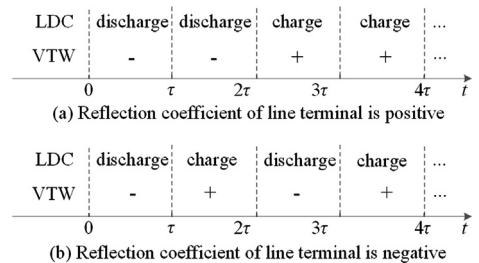


Fig. 4. Travelling wave process. (VTW represents voltage travelling wave, + and - represents positive and negative respectively).

3.1. Start-up component

The start-up component is proposed to activate the protection, and its criterion is

$$|\Delta i_\varphi| > k_1 \cdot I_n \quad \text{or} \quad |i_\varphi| > k_2 \cdot I_n \quad (9)$$

where i_φ is the measured current of the positive pole or the negative pole; Δi_φ is the sudden-change component of current, which is the difference between the current and its value of 1 ms ago. I_n is the rated current of the protected line. k_1 and k_2 are pre-fixed threshold coefficients.

The sensitivity is the key to start-up components. The threshold coefficients should ensure that the start-up criterion can be met during internal faults. Additionally, these threshold coefficients should stay away load fluctuations. In this paper, k_1 is set as 0.1, and k_2 is set as 1.1.

3.2. Fault-type component

The proposed protection is aimed at pole-to-pole faults. Pole-to-ground faults do not cause severe overcurrent in the high resistance grounding system, and the above analyses are not suitable for the pole-to-ground faults. Therefore, a criterion is proposed to distinguish fault types. During pole-to-pole faults, voltages of both poles decrease. During pole-to-ground faults, the voltage of the fault pole decreases, while the voltage of the non-fault pole increases. The following criteria are proposed:

$$\begin{cases} |u_p| < k_3 \cdot U_n \\ |u_n| < k_3 \cdot U_n \end{cases} \quad (10)$$

where u_p and u_n are the measured voltages of the positive pole and the negative pole, respectively; U_n is the rated pole voltage; k_3 is a pre-fixed threshold coefficient.

The threshold coefficient k_3 should stay away the voltage during the pole-to-ground faults. Under normal conditions, the pole voltage is expected between $0.95U_n$ and $1.05U_n$. During pole-to-ground faults, the non-fault pole voltage is larger than $0.95U_n$. Therefore, k_3 is set as 0.95, which can identify pole-to-pole faults.

It should be noticed that for a solid grounding system, the proposed protection is also suitable for pole-to-ground faults, and the fault-type component is no longer needed.

3.3. Internal fault component

The differential current is defined as the sum of the currents of both ends of the protected line.

$$i_{cd} = i_M + i_N \quad (11)$$

where i_{cd} is the differential current; i_M and i_N are respectively the currents at both ends, whose positive direction is from bus to line.

The ratio of the low-frequency energy to the high-frequency energy of the differential current is adopted to identify internal faults:

$$E_L/E_H > k_4 \quad (12)$$

where E_L and E_H are respectively the energy of low-frequency (below 1.56 kHz) and high-frequency (above 1.56 kHz); k_4 is a pre-fixed threshold. The method obtaining E_L and E_H will be shown in the next Section of signal processing.

The data window and the threshold k_4 are two critical factors for the performance of the protection.

Calculations of the energy needs a data window. The length of the data window will affect the speed and the sensitivity of the protection. A short data window can reduce the operation time of the protection. For the proposed protection, the fault current is the operation component, and the LDC current is the brake component. After the fault inception, the fault current increases and the LDC current decays. A long data window can ensure that the protection sensitively operates during

internal faults. With the system parameters of this paper, the fault current reaches its peak within 2 ms. According to the above analysis, the data window length is set as 2 ms in this paper.

The threshold k_4 will affect the reliability and the sensibility of the protection. During external faults, synchronisation errors might cause the error of differential current. A high threshold can prevent protection from maloperation caused by synchronisation errors. A low threshold can improve the sensitivity of the protection. Normally, the threshold k_4 is recommended to be set as 1.

3.4. Dead zone component

For the faults located at the near-end, the frequency of the fault current during the discharging stage might be above 1.56 kHz. In theory, there is a near-end dead zone for the internal fault criterion (12). With the system parameters of this paper, the dead zone range is from 0 km to 0.158 km. Therefore, a dead zone criterion is needed to prevent protection from miss trip in the dead zone. The dead zone criterion is:

$$\begin{cases} du/dt > k_5 \\ i_\varphi > 1.1 \times I_n \end{cases} \quad (13)$$

where du/dt is the rate of change of the pole-to-pole voltage. k_5 is a threshold. i_φ is the measured current, and I_n is the rated current that is a positive value.

The threshold k_5 should stay away the rate of change of the pole-to-pole voltage during the external faults in the remote adjacent line. It can be set with simulations, in which a solid fault is located at the outlet of the remote adjacent line.

This dead zone criterion can cover the near-end dead zone and do not exceed the protected line.

3.5. Protection logic

The protection logic is shown in Fig. 5. After the inception of faults, the protection is activated by the start-up component. Then, if the fault-type criteria are met, the data of the differential current within 2 ms after start-up are extracted. DWT is adopted to analyse the frequency characteristics of the differential current. The results of DWT are utilised by the internal fault component. If the internal fault criterion is met, the protection operates. At the same time, if the dead zone criteria are met, the protection also trips.

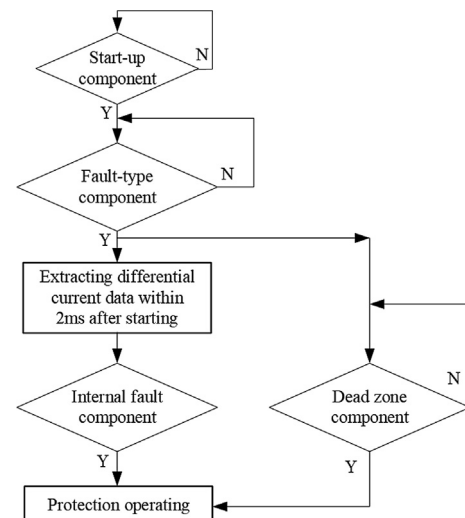


Fig. 5. Flowchart of the proposed algorithm.

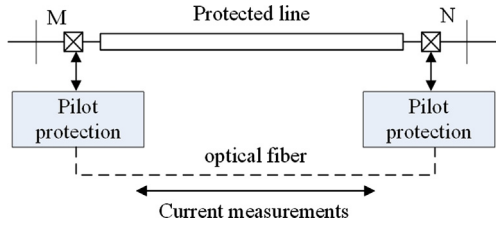


Fig. 6. Schematic diagrams of protection installation.

3.6. Protection installation

The schematic diagram of the protection installation is shown in Fig. 6. There are two protective relays installed at the both terminals of the protected line. The two protective relays exchange their current measurements with each other through optical fibres. Generally, Hall-effect transducers are adopted to measure the DC current signal.

4. Signal processing

4.1. Discrete wavelet transform

The wavelet transform is one of the powerful tools for processing signals. It has good localisation performance in both time and frequency domains and is efficient for both high-frequency and low-frequency signals.

Discrete Wavelet Transform (DWT) [35] can divide signals into different frequency bands according to a certain scale, and then reconstruct the time-domain signals to separate each frequency band. As shown in Fig. 7, for a signal whose sampling frequency is 50 kHz, 4-layer decompositions and reconstructions are implemented. The high-frequency time-domain signals (1.56–25 kHz) are extracted. Therefore, DWT is chosen to process the differential current signals.

4.2. Selection of mother wavelet

The mother wavelet is crucial to the performance of wavelet transform. Its selection is still a difficult problem. This paper proposes a method to select mother wavelet for the analysis of differential current.

The general idea is to select the mother wavelet which can genuinely reflect the frequency distribution characteristics. The specific steps are as follows:

First step: proposing digital signals to simulate the differential current during each fault stage.

For the discharging stage, the differential current involves decaying periodic components (low-frequency) and LDC current (high-frequency). The digital signal of (14) is adopted.

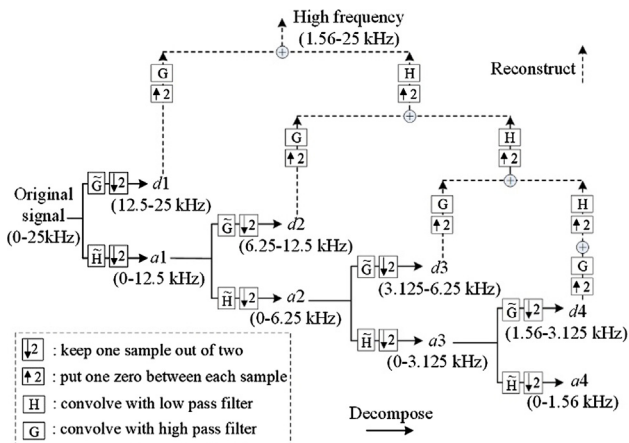


Fig. 7. Decomposition and reconstruction of DWT.

$$x_c(t) = e^{-150t} \cos(2\pi \times 500 \times t) + e^{-150t} \sin(2\pi \times 500 \times t) - \cos(2\pi \times 3000 \times t) \quad (14)$$

For the free-wheeling stage, the differential current includes decaying DC component and LDC current. The following signal is used.

$$x_d(t) = e^{-300t} - \cos(2\pi \times 3000 \times t) \quad (15)$$

For the feeding stage, the differential current mainly contains 6th harmonic components and LDC current, which is simulated with the following signals.

$$x_f(t) = \cos(2\pi \times 300 \times t) - \cos(2\pi \times 3000 \times t) \quad (16)$$

Second step: for the above digital signals of each stage, extracting their low-frequency signal and high-frequency signal with candidate mother wavelet; and calculating their energies. Then, the frequency band extraction error is defined as

$$\lambda_i = 100 \times \left| \frac{E_{L\text{signal}}}{E_{H\text{signal}}} - \frac{E_{L\text{wavelet}}}{E_{H\text{wavelet}}} \right| / \frac{E_{L\text{signal}}}{E_{H\text{signal}}} \quad (17)$$

where the subscript i represents the fault stage; $E_{L\text{wavelet}}$ and $E_{H\text{wavelet}}$ is respectively the energy of low-frequency and high-frequency extracted by the candidate mother wavelet; $E_{L\text{signal}}$ and $E_{H\text{signal}}$ are respectively the actual energy of low-frequency and high-frequency of the digital signals. The energy is calculated as

$$E = \int_0^T x(t)^2 dt \quad (18)$$

Third step: calculating the weighted error coefficient ξ of the candidate mother wavelet with (19). The error coefficient involves the frequency band extraction errors of each fault stage and the computational complexity of the candidate mother wavelet. The mother wavelet whose error coefficient is minimum will be selected for the proposed protection.

$$\xi = w_1 \cdot \lambda_c + w_2 \cdot \lambda_d + w_3 \cdot \lambda_f + w_4 \cdot C_{\text{wavelet}} \quad (19)$$

where λ_c , λ_d , and λ_f is the frequency band extraction error of discharging stage, free-wheeling stage, and feeding stage respectively; C_{wavelet} represents the computational complexity of the candidate mother wavelet; w_{1-4} represents the respective weights.

The computational complexity C_{wavelet} is defined as

$$C_{\text{wavelet}} = 100 \times \frac{T_{\text{wavelet}} - T_{\text{db1}}}{T_{\text{db1}}} \quad (20)$$

where T_{wavelet} is the calculation time of the candidate mother wavelet (this paper adopts the total time of 50,000 calculations), and T_{db1} is the calculation time of db1 mother wavelet. C_{wavelet} is a relative complexity of candidate mother wavelet compared to db1.

The weights w_{1-4} are important. The selection of weight values is based on the possibility of the fault stage appearing in the protection data window. To the DC system shown in the Fig. 1, the DC fault process involves the three stages in most cases. The protection proposed in this paper is expected as a primary protection, which should operate within a couple of milliseconds. The data window of wavelet transform involves mainly the capacitor discharging stage that is the initial fault stage. Therefore, the weight of the discharging stage w_1 should be much bigger than the other weights, which is set as 0.8. The second stage and the third stage are given small weights, 0.1 and 0.05 respectively. The computational complexity C_{wavelet} is related to the computing ability of protection, which is not the key problem to the protection with DSP (Digital Signal Processing). The computational complexity is also given a small weight of 0.05. The weight setting can also be adjusted if the wavelet transform is used for other purpose.

Table 1 lists the error calculation results of the candidate mother wavelets (db1 to db10 and sym1 to sym10). As shown in the table, the

Table 1
Extraction errors of candidate mother wavelets.

| Mother wavelet | λ_c | λ_d | λ_f | C_{wavelet} | ξ_{wavelet} |
|----------------|-------------|-------------|-------------|----------------------|------------------------|
| db1 | 15.06 | 11.81 | 37.93 | 0 | 15.13 |
| db2 | 10.63 | 7.46 | 8.19 | 2.44 | 9.78 |
| db3 | 10.78 | 6.03 | 8.33 | 4.74 | 9.88 |
| db4 | 0.57 | 4.20 | 9.41 | 5.20 | 1.61 |
| db5 | 1.15 | 1.07 | 5.26 | 6.25 | 1.60 |
| db6 | 7.40 | 3.08 | 5.21 | 5.27 | 6.75 |
| db7 | 3.80 | 0.43 | 3.91 | 9.51 | 3.75 |
| db8 | 0.52 | 2.37 | 4.00 | 9.52 | 1.33 |
| db9 | 11.55 | 6.22 | 0.49 | 8.58 | 10.32 |
| db10 | 1.36 | 0.35 | 5.55 | 9.36 | 1.87 |
| sym1 | 15.06 | 11.81 | 37.93 | 14.48 | 15.85 |
| sym2 | 10.63 | 7.46 | 8.19 | 0.87 | 9.70 |
| sym3 | 10.78 | 6.03 | 8.33 | 2.20 | 9.75 |
| sym4 | 7.69 | 3.58 | 5.07 | 2.44 | 6.89 |
| sym5 | 3.04 | 4.42 | 2.17 | 3.79 | 3.17 |
| sym6 | 3.49 | 0.27 | 3.23 | 4.20 | 3.19 |
| sym7 | 1.44 | 1.04 | 3.12 | 5.14 | 1.67 |
| sym8 | 1.49 | 0.44 | 1.90 | 5.76 | 1.62 |
| sym9 | 3.73 | 2.53 | 0.45 | 436.85 | 25.10 |
| sym10 | 3.53 | 2.45 | 0.30 | 785.38 | 42.35 |

extraction errors of the different mother wavelet are different. The weighted error coefficient of db8 mother wavelet is minimum. Therefore, the db8 mother wavelet is adopted to process the differential current signal for the proposed protection.

5. Simulation verification

A model of a double-terminal DC distribution simulation system (as shown in Fig. 1) has been constructed in PSCAD/EMTDC to verify the proposed algorithms. The DC rated voltage is ± 10 kV, and the rated capacities of the VSCs are 7 MW. The DC-side voltage is controlled by VSC1, and VSC2 controls the active power. The AC rated voltage is 10 kV, and the short-circuit capacity is 350 MVA. The fundamental frequency of the AC system is 50 Hz. The AC-side equivalent inductances are 10 mH. The DC-link capacitors are 100 μ F. The DC-side is grounded by a high resistance.

There are three sections of DC lines whose length are all 5 km, which are simulated with π -type equivalent circuits, and their parameters are shown in Table 2.

The MN line is taken as an example to verify the proposed protection. The protection relays are installed at both M and N terminals. Point-to-point optical-fibre channels are utilised by the protections to exchange data.

The proposed protection can use different sampling frequencies, such as 10 kHz or 50 kHz which have been applied in real projects. With different sampling rate, the number of decomposition layers and the data window should be adjusted accordingly. Consistent with the previous analyses, the sampling frequency adopted in this simulation is 50 kHz.

5.1. Internal pole-to-pole faults

5.1.1. Solid faults

A pole-to-pole solid fault was located at the midpoint of MN Line at 0 ms. The original differential current is shown in Fig. 8(a). The low-

Table 2
DC cable parameters.

| Resistance | Self-inductance | Mutual inductance | Capacitance to earth | Coupling capacitance |
|--------------------|-----------------|-------------------|----------------------|----------------------|
| 0.125 Ω /km | 0.586 mH/km | 0.256 mH/km | 0.350 μ F/km | 0.039 μ F/km |

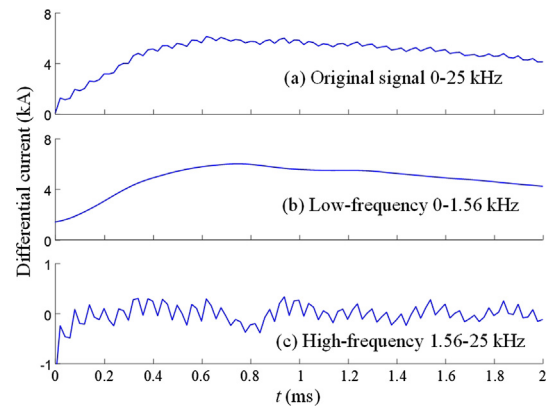


Fig. 8. Differential current during internal pole-pole fault.

frequency (0–1.56 kHz) time-domain signal of the differential current is shown in Fig. 8(b), which is extracted with DWT whose mother wavelet is db8. The high-frequency (1.56–25 kHz) time-domain signal is shown in Fig. 8(c). The low-frequency energy is 49902.70 $A^2 \cdot s$, and the high-frequency energy is 98.17 $A^2 \cdot s$. The ratio of low-frequency to high-frequency is 508.30, which is much larger than 1. The internal fault criterion (12) is met, which means that the differential current mainly contains the fault currents. The protection operates correctly.

The pole-to-pole solid faults were also tested under different fault distance as shown in Table 3. When the fault is located at 0% of the MN Line, the proposed internal fault component cannot be activated, that is called Dead Zone. The proposed dead zone component (13) can be met in that case, and the protection still operates correctly. For the other faults in the table, the internal fault component is activated, and the protection operates correctly. Therefore, it is justified that the proposed protection can cover the whole protected line.

5.1.2. Faults with resistance

On the aspect of sensitivity, the influences of fault distance are evaluated. Pole-to-pole faults with fault resistances at the midpoint of MN Line were simulated to test the proposed protection. The test results are shown in Table 4. For the faults with the resistance from 0.1 to 50 Ω , the internal fault component can be activated, and the protection operates correctly. It should be noticed that the fault resistance does not reduce the sensitivity of the protection. There are two reasons for this. One reason is that both the fault current and the LDC current decrease as the fault resistance increases. The proposed protection is based on their ratio. The other reason is that the fault resistance decreases the speed of the start-up component. The increase in the fault resistance causes the data window of the internal fault component to move backward, which might increase the sensitivity of the protection.

Table 3
Test results under different fault distance.

| Fault distance | $E_I/(A^2 \cdot s)$ | $E_{II}/(A^2 \cdot s)$ | E_I/E_{II} | Behavior |
|----------------|---------------------|------------------------|--------------|----------|
| 0% | 32161.48 | 145711.43 | 0.22 | DZ OP |
| 10% | 164675.18 | 996.46 | 165.26 | IF OP |
| 20% | 95102.63 | 215.03 | 442.27 | IF OP |
| 40% | 57570.12 | 100.77 | 571.28 | IF OP |
| 50% | 49902.70 | 98.17 | 508.30 | IF OP |
| 60% | 45104.88 | 69.47 | 649.27 | IF OP |
| 80% | 38808.00 | 77.01 | 503.95 | IF OP |
| 90% | 37187.95 | 76.65 | 485.14 | IF OP |
| 100% | 35661.83 | 57.07 | 624.85 | IF OP |

Notes: DZ OP represents that Dead zone component operates; IF OP represents that internal fault component operates. The fault distance is calculated from M terminal, and 100% represents the whole MN Line.

Table 4
Test results under internal faults with resistance.

| Fault resistance | $E_L/(A^2\cdot s)$ | $E_H/(A^2\cdot s)$ | E_L/E_H | Behavior |
|------------------|--------------------|--------------------|-----------|----------|
| 0.1 Ω | 45363.21 | 93.71 | 484.10 | IF OP |
| 2 Ω | 14011.05 | 50.39 | 278.06 | IF OP |
| 5 Ω | 6833.20 | 30.56 | 223.62 | IF OP |
| 10 Ω | 3301.18 | 4.44 | 742.83 | IF OP |
| 15 Ω | 1950.09 | 1.84 | 1060.25 | IF OP |
| 20 Ω | 1292.13 | 0.77 | 1681.90 | IF OP |
| 30 Ω | 689.66 | 0.14 | 4929.89 | IF OP |
| 40 Ω | 427.15 | 0.17 | 2459.84 | IF OP |
| 50 Ω | 286.52 | 0.35 | 811.01 | IF OP |

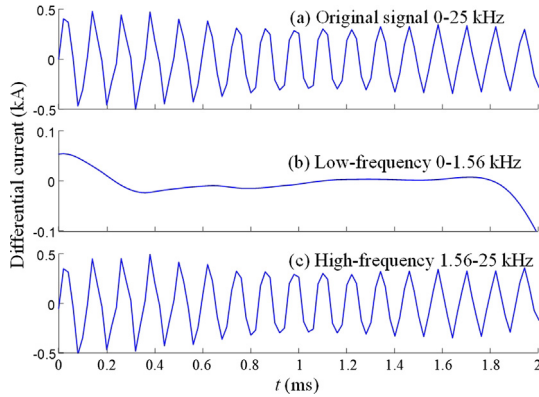


Fig. 9. Differential current during external pole-pole fault.

5.2. External pole-to-pole faults

5.2.1. External faults

A pole-to-pole solid fault was located at the outlet of the adjacent line, which is an external fault for the protection of MN Line. The protection is not expected to operate. The differential current of MN Line is shown in Fig. 9. The low-frequency energy is 1.23 A²s, and the high-frequency energy is 130.65 A²s. The ratio of low-frequency to high-frequency is 0.01, which is far less than 1. Neither the internal fault criterion (12) nor the dead zone component (13) can be met. The differential current mainly contains the LDC currents. The protections do not trip.

The external faults with resistance also are tested to assess the selectivity of the protection, as shown in Table 5. Though, the energy of high-frequency decreases following the increase of the fault resistance, it is still larger than the low-frequency energy during the external faults. For the external faults with the resistances from 0.1 to 50 Ω , the protections of MN do not trip. The external faults cannot cause the maloperation of the proposed protection, which shows excellent reliability.

5.2.2. Influence of noise

On the aspect of the reliability, the white noise was superimposed

Table 5
Test results under external faults with resistance.

| Fault resistance | $E_L/(A^2\cdot s)$ | $E_H/(A^2\cdot s)$ | E_L/E_H | Behavior |
|------------------|--------------------|--------------------|-----------|----------|
| 0.1 Ω | 1.09 | 119.96 | 0.01 | No trip |
| 2 Ω | 0.53 | 38.95 | 0.01 | No trip |
| 5 Ω | 0.50 | 15.41 | 0.03 | No trip |
| 10 Ω | 0.44 | 6.36 | 0.07 | No trip |
| 15 Ω | 0.36 | 3.46 | 0.11 | No trip |
| 20 Ω | 0.29 | 2.14 | 0.14 | No trip |
| 30 Ω | 0.18 | 0.96 | 0.18 | No trip |
| 40 Ω | 0.11 | 0.50 | 0.21 | No trip |
| 50 Ω | 0.06 | 0.29 | 0.21 | No trip |

Table 6
Test results under external faults with noise.

| SNR | $E_L/(A^2\cdot s)$ | $E_H/(A^2\cdot s)$ | E_L/E_H | Behavior |
|-------|--------------------|--------------------|-----------|----------|
| 60 dB | 1.24 | 130.74 | 0.010 | No trip |
| 50 dB | 1.21 | 131.34 | 0.009 | No trip |
| 40 dB | 1.14 | 135.56 | 0.008 | No trip |
| 30 dB | 1.41 | 151.83 | 0.009 | No trip |
| 20 dB | 3.39 | 377.90 | 0.009 | No trip |

on the measurements of the external fault whose current has been shown in Fig. 9. The results with noises are shown in Table 6. Because the noise is a high-frequency signal that is a brake component for the proposed protection, the noise cannot cause maloperations during external faults in principle. As Table 6 shown, the high-frequency energy increases with noise, which improves the reliability of the protection during external faults. The protection can withstand the interference of noise up to 20 dB.

5.2.3. Influence of synchronisation error

The synchronisation methods [36] generally used for differential protection involve the ping-pong scheme and the GPS method. The synchronisation error of the ping-pong scheme is related to the time delay difference between the receiving and transmitting channels, which is relatively small for a point-to-point optical-fibre channel. The synchronisation error of the GPS method is within 2 μ s [37].

The synchronisation error will lead to the error of the differential current, which affects the performance of the proposed protection. The test results under synchronisation errors are shown in Table 7. The synchronisation errors were superimposed on the external solid fault, and the protection is not expected to trip. As shown in Table 7, the protection does not trip in mistake if the synchronisation error is less than 40 μ s, which is generally met for the GPS method. For the ping-pong scheme, in the distribution network, the time delay difference between the receiving and transmitting channels is generally less than 40 μ s in the case of point-to-point optical-fibre.

For situations where the synchronisation error is huge, the maloperation of the protection can be prevented by increasing the threshold of E_L/E_H , which might reduce the sensitivity of protection.

5.2.4. Influence of line length

To indicate the effectiveness of the proposed protection for the different line parameters, the test results under different line lengths are shown in Table 8. In these tests, a solid fault is located at the middle of the protected line for these internal faults, while a solid fault is located at the outlet of the next line for these external faults. From these results, under different line lengths, the protection always has its good sensitivity and reliability to the setting of E_L/E_H that is set as 1.

5.3. Pole-to-ground faults

A positive-pole-to-ground fault was located at the midpoint of MN at 0 ms. Because of the grounding style of the DC system, the pole-to-ground faults cannot cause severe overcurrent, and the DC system can keep operating to enhance the supply reliability. As shown in Fig. 10, the voltage of the positive pole (fault pole) decays, and the absolute

Table 7
Test results under synchronisation error during an external fault.

| Synchronisation error | $E_L/(A^2\cdot s)$ | $E_H/(A^2\cdot s)$ | E_L/E_H | Behavior |
|-----------------------|--------------------|--------------------|-----------|------------|
| 20 μ s | 7.30 | 109.25 | 0.067 | No trip |
| 40 μ s | 18.93 | 49.77 | 0.381 | No trip |
| 60 μ s | 38.36 | 0.42 | 91.857 | maloperate |
| 80 μ s | 67.32 | 51.67 | 1.303 | maloperate |

Table 8
Test results under different line lengths.

| Line length | Fault location | $E_L/(A^2\cdot s)$ | $E_H/(A^2\cdot s)$ | E_L/E_H | Behavior |
|-------------|----------------|--------------------|--------------------|-----------|----------|
| 1 km | Internal | 177,101 | 943.60 | 187.69 | IF OP |
| 1 km | External | 0.0623 | 8.76 | 0.0071 | No trip |
| 3 km | Internal | 74,195 | 118.11 | 628.20 | IF OP |
| 3 km | External | 0.1485 | 100.42 | 0.0015 | No trip |
| 6 km | Internal | 43,680 | 64.27 | 679.67 | IF OP |
| 6 km | External | 1.60 | 130.04 | 0.01 | No trip |
| 8 km | Internal | 34,758 | 67.79 | 512.71 | IF OP |
| 8 km | External | 1.42 | 138.27 | 0.01 | No trip |
| 10 km | Internal | 29,303 | 78.19 | 374.79 | IF OP |
| 10 km | External | 2.33 | 147.15 | 0.02 | No trip |

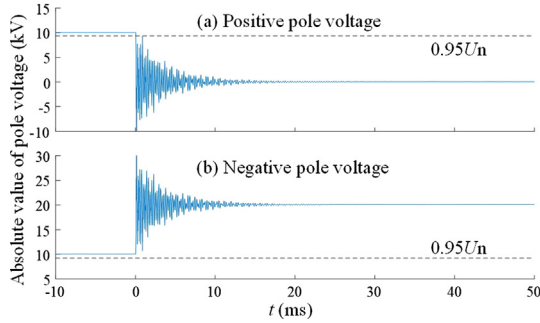


Fig. 10. Pole voltage during pole-ground fault.

value of the negative pole voltage (non-fault pole) increases. The fault-type criterion (10) cannot be met. The proposed protection does not maloperate during pole-to-ground faults.

5.4. Protection operation time

The operation time of the protection involves algorithm time and communication time. In terms of algorithm time, the data window length of the algorithm is 2 ms, and the calculation time generally does not exceed 0.5 ms using the current DSP (Digital Signal Processing) [38]. For communication time, if the dedicated fibre channel is adopted, the transmission speed of the data is about 4.9 $\mu\text{s}/\text{km}$, and, the transmission time of the channel is about 0.1 ms for lines of 20 km. With the above time and some delay, the operation time of the proposed protection is within 3 ms.

6. Discussion

The new current differential protection is proposed, which is based on the frequency instead of the magnitude in time-domain. The proposed protection will be compared to the conventional current differential protection (CCDP) as follows.

The criterion of CCDP [8], which is applied in the Xinsong-Dongfang ± 800 kV HVDC system, is shown as:

$$\begin{cases} |i_M + i_N| > 0.05 I_n \\ |i_M + i_N| > 0.1 \times |i_M - i_N| \end{cases} \quad (21)$$

For the internal faults, both the CCDP and the proposed protection can correctly operate. However, for the external faults, the proposed protection has better performances than the CCDP.

An external solid fault is located at the outlet of the adjacent line, for which the protections are not expected to operate. As shown in Fig. 11(a), at the initial stage of the fault, the differential current, which is mainly the current of LDC, exceeds the brake current. Therefore, a time delay is necessary to the CCDP. It should be noticed that the time delay increases sharply with the growth of the length of the protection line. As shown in Fig. 11(b), when the protected line is 10 km, the time

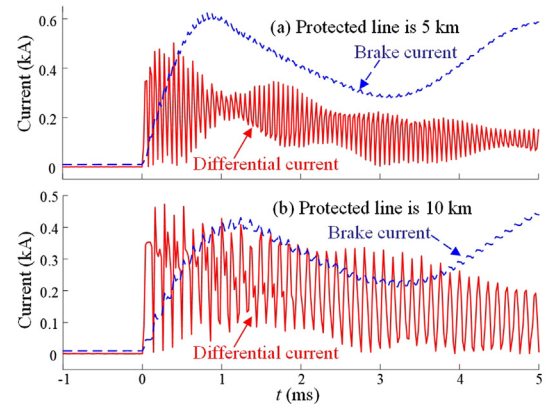


Fig. 11. Performance of CCDP under external fault. (a) Protected line is 5 km; (b) Protected line is 10 km.

delay of the CCDP is at least 4 ms. It is also the reason that the CCDP is generally adopted as a back-up protection.

The proposed protection has a data window with a fixed length, which guarantees the operation time within 3 ms. The proposed algorithm improves the performance of current differential protection, and is a potential primary protection.

The disadvantage of the proposed protection is the near-end dead zone for the internal fault criterion. The dead zone criterion has been proposed to assist the protection in handling near-end faults.

In the future research, the problem of the near-end dead zone should be further researched. Additionally, the artificial intelligence such as some heuristic methods can be introduced to select the suitable candidate of mother wavelet.

7. Conclusion

The protection technique is crucial to the safety and reliability of VSC-DC distribution systems. Aiming at the shortcoming of the current differential protection, the paper proposes an idea to identify faults with the frequency-domain information of the differential current instead of its magnitude in time-domain. The features of the proposed protection is shown as follows:

- (1) Regarding speed, the protection can trip for internal faults in less than 3 ms.
- (2) Regarding selectivity, the protection can cover the whole line, and does not maloperate for external faults.
- (3) Regarding reliability, the LDC current is the brake component for protection instead of the maloperation component. The protection can tolerate 20 dB of noises and 40 μs of synchronisation error.
- (4) Regarding sensitivity, the protection can correctly operate under fault resistance up to 50 Ω .

The main contributions of this paper are described as:

- (1) The frequency-based current differential protection is proposed, which is immune to the LDC current thoroughly and can resist the interference of noises.
- (2) A method is proposed to select a suitable mother wavelet for the DWT.
- (3) A dead zone criterion is proposed to assist the protection in handling near-end faults.

The proposed protection can meet the speed and selectivity requirement, which is the candidate of a primary protection for the VSC-MVDC distribution systems.

Declaration of Competing Interest

The authors declared that they have no conflicts of interest to this work.

We declare that we do not have any commercial or associative interest that represents a conflict of interest in connection with the work submitted.

Acknowledgments

This work was supported in part by the State's Key Project of Research and Development Plan under the Grant 2018YFB0904602, by the State Grid Corporation headquarters technology project: 'Research on Integrated Protection Design Technology of Multi-terminal Cascaded Hybrid HVDC System Based on Protection-Control-Collaboration' (No. 5200-201956113A-0-0-00).

References

- [1] Lu W, Ooi BT. Premium quality power park based on multi-terminal HVDC. *IEEE Trans Power Del* 2005;20(2):978–84.
- [2] Salomonsson D, Soder L, Sannino A. Protection of low-voltage DC microgrids. *IEEE Trans Power Del* 2009;24(3):1045–53.
- [3] Akhmatov V, Callavik M, Franck CM, et al. Technical guidelines and pre-standardization work for first HVDC grids. *IEEE Trans Power Del* 2014;29(1):327–35.
- [4] Dantas R, Liang J, Ugalde-Loo CE, et al. Progressive fault isolation and grid restoration strategy for MTDC networks. *IEEE Trans Power Del* 2018;33(2):909–18.
- [5] Mokhberdoran A, et al. Multiport Hybrid HVDC Circuit Breaker. *IEEE Trans Ind Electron* 2018;65(1):309–20.
- [6] Wu J, Li H, Wang G, et al. An improved traveling-wave protection scheme for LCC-HVDC transmission lines. *IEEE Trans Power Del* 2017;32(1):106–16.
- [7] Saleh KA, Hooshyar A, El-Saadany EF, et al. Ultra-high-speed traveling-wave-based protection scheme for medium-voltage DC microgrids. *IEEE Trans Smart Grid* 2019;10(2):1440–51.
- [8] Tong N, Lin X, Li Y, et al. Local measurement-based ultra-high-speed main protection for long distance VSC-MTDC. *IEEE Trans Power Del* 2019;34(1):353–64.
- [9] Baran ME, Mahajan NR. Overcurrent protection on voltage-source-converter-based multiterminal DC distribution systems. *IEEE Trans Power Del* 2007;22(1):406–12.
- [10] Emhemed AAS, Burt GM. An advanced protection scheme for enabling an LVDC last mile distribution network. *IEEE Trans Smart Grid* 2014;5(5):2602–9.
- [11] Saleh KA, Hooshyar A, El-Saadany EF. Hybrid passive-overcurrent relay for detection of faults in low-voltage DC grids. *IEEE Trans Smart Grid* 2017;8(3):1129–38.
- [12] Emhemed AAS, Fong K, Fletcher S, et al. Validation of fast and selective protection scheme for an LVDC distribution network. *IEEE Trans Power Del* 2017;32(3):1432–40.
- [13] Sneath J, Rajapakse AD. Fault detection and interruption in an earthed HVDC grid using ROCOV and hybrid DC breakers. *IEEE Trans Power Del* 2016;31(3):973–81.
- [14] De KK, Srivastava K, Reza M, et al. Wavelet-based protection strategy for DC faults in multi-terminal VSC HVDC systems. *IET Gener Transm Distrib* 2011;5(4):496–503.
- [15] Fletcher SDA, Norman PJ, Galloway SJ, et al. Optimizing the roles of unit and non-unit protection methods within DC microgrids. *IEEE Trans Smart Grid* 2012;3(4):2079–87.
- [16] Yang J, Fletcher JE, O'Reilly J. Multiterminal DC wind farm collection grid internal fault analysis and protection design. *IEEE Trans Power Del* 2010;25(4):2308–18.
- [17] Xiang W, Yang S, Xu L. A transient voltage-based DC fault line protection scheme for MMC-based DC grid embedding DC breakers. *IEEE Trans Power Del* 2019;34(1):334–51.
- [18] Leterme W, Beerten J, Hertem DV. Nonunit protection of HVDC grids with inductive DC cable termination. *IEEE Trans Power Deliv* 2016;31(2):820–8.
- [19] Li R, Xu L, Yao L. DC fault detection and location in meshed multiterminal HVDC systems based on DC reactor voltage change rate. *IEEE Trans Power Del* 2016;31(1):1–11.
- [20] Wang W, Barnes M, Marjanovic O, et al. Impact of dc breaker systems on multi-terminal VSC-HVDC stability. *IEEE Trans Power Del* 2016;31(2):769–79.
- [21] Takeda H, Ayakawa H, Tsumenaga M, et al. New protection method for HVDC lines including cables. *IEEE Trans Power Deliv* 1995;10(4):2035–9.
- [22] Fletcher SDA, Norman PJ, Fong K, et al. High-speed differential protection for smart DC distribution systems. *IEEE Trans Smart Grid* 2014;5(5):2610–7.
- [23] Monadi M, Gavriluta C, Luna A, et al. Centralized protection strategy for medium voltage DC microgrids. *IEEE Trans Power Del* 2017;32(1):430–40.
- [24] Park J, Candelaria J. Fault detection and isolation in low-voltage DC-bus microgrid system. *IEEE Trans Power Del* 2013;28(2):779–87.
- [25] Yining Z, Jiale S. Phaselet-based current differential protection scheme based on transient capacitive current compensation. *IET Gen Transm Distrib* 2008;2(4):469–99.
- [26] Xu ZY, Du ZQ, Ran L, et al. A current differential relay for a 1000-kV UHV transmission line. *IEEE Trans Power Del* 2007;22(3):1392–9.
- [27] Tang L, Dong X, Lou S, et al. A new differential protection of transmission line based on equivalent travelling wave. *IEEE Trans Power Del* 2017;32(3):1359–70.
- [28] Li S, Chen W, Yin X, et al. Protection scheme for VSC-HVDC transmission lines based on transverse differential current. *IET Gener Transm Distrib* 2017;11(11):2805–13.
- [29] Ooi BT, Wang X. Voltage angle lock loop control of boost type PWM converter for HVDC application. *IEEE Trans Power Electron* 1990;5(2):229–35.
- [30] Marquardt R. Stromrichterschaltungen mit verteilten energiespeichern. Germany Patent Application DE10103031A1; Jan. 2001.
- [31] Yang J, Fletcher JE, O'Reilly J. Short-circuit and ground fault analyses and location in VSC-based DC network cables. *IEEE Trans Ind Electron* 2012;59(10):3827–37.
- [32] Li M, Jia K, Bi T, et al. Sixth harmonic-based fault location for VSC-DC distribution systems. *IET Gener Transm Distrib* 2017;11(14):3485–90.
- [33] He Z, Liao K, Li X, et al. Natural frequency-based line fault location in HVDC lines. *IEEE Trans Power Del* 2014;29(2):851–9.
- [34] Li R, Sun L, Zhang H, et al. Research on DC voltage class series with AHP. *J Eng* 2017;2017(13):1993–8.
- [35] Mallat SG. 'A theory for multiresolution signal decomposition: the wavelet representation'. *IEEE Trans Pattern Anal Mach Intell* 1989;11(7):674–94.
- [36] Jin N, Lin X, Xing J, et al. Research on multi-terminal current differential protection criterion with high sensitivity and synchronisation error tolerance capability. *IEEE Trans Power Del* 2017;32(3):1359–70.
- [37] Villamagna N, Crossley PA. A symmetrical component-based GPS signal failure-detection algorithm for use in feeder current differential protection. *IEEE Trans Power Del* 2008;23(4):1821–8.
- [38] Darwish HA, Hesham M, Taalab AI, et al. Close accord on DWT performance and real-time implementation for protection applications. *IEEE Trans Power Del* 2012;25(4):2174–83.